Encrypted Simultaneous Control of Joint Angle and Stiffness of Antagonistic Pneumatic Artificial Muscle Actuator by Polynomial Approximation

Yuta Takeda, *Student Member, IEEE*, Takaya Shin, Kaoru Teranishi, *Student Member, IEEE*, and Kiminao Kogiso, *Member, IEEE*

***Abstract*—This study proposes an encrypted simultaneous control system for an antagonistic pneumatic artificial muscle (PAM) actuator to develop a cybersecure and flexible actuator. First, a simultaneous control system design is considered for the joint angle and stiffness of a PAM actuator in a model-based design approach, thus facilitating the use of an encrypted control method. The designed controller includes a contraction force model expressed as rational polynomial functions, which makes it difficult to encrypt the controller. To overcome this difficulty, a least absolute shrinkage and selection operator-based polynomial approximation is employed for a rational controller. Then, the resulting polynomial controller is transformed into a matrix-vector product form, which enables the use of a specific homomorphic encryption scheme to develop an encrypted simultaneous control system for the PAM actuator. Finally, this study quantitatively evaluates the tracking control performance of the original, approximated, and encrypted controllers. The experimental results show that the proposed encrypted controller achieves simultaneous tracking of the joint angle and stiffness with a tracking error of less than 3.7%.**

***Index Terms*—Encrypted control, experimental validation, least absolute shrinkage and selection operator (LASSO), pneumatic artificial muscle (PAM), polynomial-type controller, simultaneous control.**

I. Introduction

THE McKibben pneumatic artificial muscle (PAM) was first developed in the 1950s [1]. A PAM is inflated by injecting compressed air into a rubber tube wrapped in a non-stretchable mesh to generate a contraction force. This structure offers several advantages over traditional motors and cylinders, including compact size, lightweight, and flexibility [2], [3]. Because PAMs produce contraction force in a single direction, an antagonistic configuration is typically adopted for practical applications, where two PAMs are arranged in parallel through joints [4], [5]. This structure facilitates rotational motion and closely mimics human movements [3]. Owing to these benefits, a review paper [6] stated that PAMs have found considerable use in the development of rehabilitation and assistive devices that can be comfortably worn and operated by users. Furthermore, numerous studies have explored stiffness or compliance control [7], [8], [9], [10], [11] and developed methods of simultaneous control of the joint angle and stiffness to leverage the potential of PAMs fully [12], [13], [14], [15], [16], [17]. These active controls enhance safety during contact and collision between robots and humans or their environments while also augmenting the comfort of wearable devices.

Applications that integrate wireless network technology into PAM actuator systems include remote surgical robots [18], remotely operated cranes [19], teleoperation of pneumatic robots [20], and walking-assistive devices [21], [22]. The use of wireless communications enhances the portability of devices and promotes the self-rehabilitation of patients at home. In self-rehabilitation, the monitoring of wearable devices through a network by physical therapists helps prevent injury due to falls. Meanwhile, attention must be paid to the cybersecurity of networked actuator systems. Cyberattack incidents and risk analyzes have been reported, such as the falsification of control parameters by Stuxnet to destroy process plants [23], an unmanned aerial vehicle compromised by hijacking video streaming [24], and the compromising of a robot controller [25].

To develop secure PAM actuator systems, networked actuator systems must be equipped with cybersecurity countermeasures. Encrypted control was proposed as a cyberserucrity countermeasure for networked control systems in [26] by integrating the homomorphism of a specific public-key encryption scheme into a linear or polynomial-type control system. Encrypted control conceals the control parameters inside the control device and the signals over the communication links, resulting in protection against eavesdropping [26], [27], [28], [29] and real-time detection of cyberattacks [26], [30], [31]. Encrypted implementation is expected to enhance the cybersecurity of control systems.

However, designing a nonlinear controller that is not a polynomial, such as a rational polynomial or switching controller,

Manuscript received 9 November 2023; revised 27 March 2024; accepted 30 April 2024. Recommended by Technical Editor J. Zhang and Senior Editor Y.-J. Pan. This work was supported by the JSPS KAKENHI under Grant JP22H01509 and Grant JP21K19762. *(Corresponding author: Kiminao Kogiso.)*

Yuta Takeda, Kaoru Teranishi, and Kiminao Kogiso are with the Department of Mechanical and Intelligent Systems Engineering, The University of Electro-Communications, Tokyo 1828585, Japan (e-mail: yutatakeda@uec.ac.jp; kogiso@uec.ac.jp).

Takaya Shin is with DAIHEN, Inc., 2-1-11 Tagawa, Yodogawa, Osaka, Osaka 532-8512, Japan.

Color versions of one or more figures in this article are available at https://doi.org/10.1109/TMECH.2024.3405189.

Digital Object Identifier 10.1109/TMECH.2024.3405189

is difficult. A simultaneous control system for the joint angle and stiffness of an antagonistic PAM actuator uses a rational polynomial-type controller [12], [15], [16]. In addition, encrypted proportional-integral (PI) control of the PAM joint angle or torque was considered in [29], and in [32], the implementation of encrypted polynomial controllers was demonstrated, verifying its effectiveness through a numerical toy example. Unfortunately, to the best of authors' knowledge, no studies have been conducted on encrypting such nonlinear controllers.

This study aims to propose an encrypted simultaneous control system for an antagonistic PAM actuator to develop a cyber-secure and flexible actuator. In this study, the simultaneous tracking control of the joint angle and stiffness of the antagonistic PAM actuator is considered for a step-like and sinusoidal reference. We present a model-based nonlinear control system comprising three components: a reference generator, a contraction force estimator, and PI controllers. However, a model-based controller includes specific rational functions, and application of the encrypted control method is challenging. To overcome this difficulty, this study approximates the designed controller as a polynomial-type controller that is friendly to controller encryption. Then, to evaluate the developed encrypted control system, we quantitatively investigate the effects of polynomial approximation and controller encryption on the control performance. Finally, an experimental investigation confirms that the proposed encrypted control system enables simultaneous tracking to the step-like and sinusoidal references within an acceptable tracking error. This study advances beyond [33] by redesigning the polynomial-type controller and implementing the encrypted controller.

This study makes the following two main contributions. It is the first to present an encrypted nonlinear control system for simultaneously tracking the joint angle and stiffness of an antagonistic PAM actuator. The encryption of polynomial controllers was discussed in [32], while it addressed a numerical toy example rather than practical applications. In contrast, this study addresses a practical application. Furthermore, this study provides a comprehensive controller description involving a reasonable contraction force model, which was not detailed in [33], and a modified and improved method for polynomial determination to facilitate the implementation of an encrypted controller. The provision helps reduce the number of approximations that cause control performance degradation throughout the controller encryption procedure. In addition, the controller design methods for antagonistic PAM actuators presented in [17], [33], and [34] did not employ such an encryption-awareness design policy.

The rest of this article is organized as follows. Section II introduces the antagonistic PAM actuator with a control objective and presents a model-based simultaneous control method for tracking the joint angle and stiffness of the PAM actuator to the reference. Section III discusses the polynomial approximation to acquire a friendly form of the controller to realize the encrypted control. Section IV proposes an encrypted-controlled PAM actuator to maintain the controller and communication secrets and investigates the impact of the secure implementation on the control performance to highlight the effectiveness of the proposed encrypted controller. Finally, Section V concludes this article.

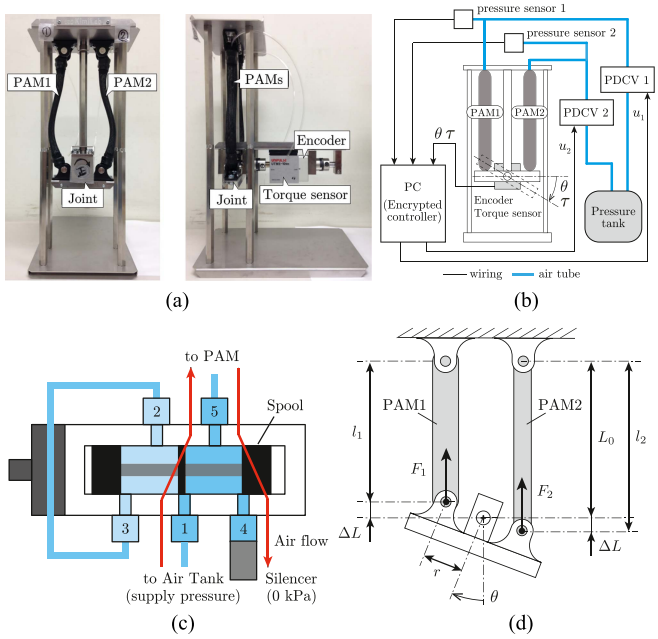

Fig. 1. Antagonistic PAM actuator system considered [34]. (a) Front and side views of antagonistic PAM actuator. (b) Schematic of the antagonistic PAM actuator system to be developed. (c) Pneumatic circuit schematic of the PDCV. (d) Illustration of PAM joint [17].

II. Nonlinear Control System Design for Antagonistic PAM Actuator

This section introduces the antagonistic PAM actuator, its simultaneous control system design, and the numerical evaluation of the control performance of the designed control system.

A. Antagonistic PAM Actuator System

An antagonistic PAM actuator is a joint actuatc in Fig. 1(a). One side of each PAM is connected by a joint. The system consists of two PAMs, two proportional directional control valves (PDCVs), an air tank, pressure sensors, a torque meter, a rotary encoder, and a control PC. The tank stores compressed air connected to the PDCVs and PAMs using air tubes. The airflow regulated by the PDCVs drives the PAMs, and the joint rotates. The system inputs are the voltage commands to the two PDCVs (u_1 and u_2), and the measured values are the joint angle θ, torque τ, and inner pressure of the PAMs (P_1 and P_2), as shown in Fig. 1(b). The range of the rotation angle is $\pm 25°$, and the range of the output torque is ± 3.0 N $\cdot$ m. The sampling period T_s was set to 4.0 ms. Table I lists the details of the experimental equipment used. Moreover, the schematic of the valve is shown in Fig. 1(c). The valve has five ports: Ports 1, 4, and 5 are connected via air tubes to the air tank, a silencer, and the PAM, respectively, while the others are not used.

The control objective considered in this study is to track the joint angle and stiffness of the PAM actuator simultaneously with respect to a given reference. The goal of this study is to develop

TABLE I
EXPERIMENTAL EQUIPMENTS

Name	Specifications
PAM	AirMuscle, Kanda Tsushin Kogyo, Length: 170 mm (be given a 2 kgf mass), Diameter: 0.5 inches.
Valve (PDCV)	5/3-way valve, FESTO, a critical frequency of 125 Hz.
Torque sensor	UTM II-10 Nm(R), UNIPULSE, range: $\pm$10 Nm.
Encoder	UTM II-10 Nm(R), UNIPULSE, Incremental, resolution: 2000 P/R
Pressure sensor	E8F2-B10C, OMRON, Range: 0–1 MPa.
Air compressor	6-25, JUN-AIR, Tank: 25 L; displacement: 60 L/min.
Pressure tank	AST-25G, EARTH MAN, 25 L.
PC	Ubuntu12.04, Xenomai2.6.2.1 Patch, CPU: 3.2 GHz, memory: 8 GB.

an encrypted simultaneous tracking control system for the joint angle and stiffness of a PAM actuator to mitigate the control performance degradation caused by secure implementation. The control problem considered in this study is as follows.

Problem 1: For the antagonistic PAM actuator system, presented in Fig. 1(a), with given references to joint angle $\bar{\theta}$ and stiffness $\bar{K}_P$, design an encrypted simultaneous controller to achieve satisfactory tracking control performance, i.e., for a sufficiently small number $\epsilon > 0$, $|\bar{\theta} - \theta(k)| < \epsilon$, and $|\bar{K}_P - K_P(k)| < \epsilon$ hold as $k \to \infty$, where $k \in \mathbb{Z}^+ := \{0, 1, 2, \ldots\}$

Remark 1: The previous study [33] primarily focused on the reasonable approximation of polynomial controllers using LASSO. However, it did not delve into the design and implementation of encrypted controllers and their evaluation, which are the main subjects of this study.

B. Joint Stiffness

Joint stiffness is an index representing the difficulty of a joint rotating against external forces [16], [17]. This study employs the model of joint stiffness, as shown in Fig. 1(d), presented in [17], following the introduction of the notations of the physical variables regarding the PAM. The lengths of the two PAMs, l_1 and l_2, are, respectively, given by $l_1(k) = L_0 - \Delta L(k)$ and $l_2(k) = L_0 + \Delta L(k)$, where $\Delta L(k) \approx r \sin\theta(k)$ is the horizontal displacement of the two PAMs, r is the radius of the joint, and L_0 is the PAM length when the joint is at the horizontal position. The contraction force of the PAM $F_i, \forall i \in \mathcal{I} := \{1, 2\}$ can be expressed as a function of the inner pressure and length as follows:

$$F_i(l_i(k), P_i(k)) = a_i(l_i(k))P_i(k) + b_i(l_i(k)) \quad \forall i \in \mathcal{I} \quad (1)$$

where $P_i(k), \forall i \in \mathcal{I}$ is the inner pressure, $a_i(l_i(k)) \approx p_i^{a_1} l_i(k) + p_i^{a_2} = p_i^{a_1}(L_0 \mp r\sin\theta(k)) + p_i^{a_2}$ and $b_i(l_i(k)) \approx p_i^{b_1} l_i(k) + p_i^{b_2} = p_i^{b_1}(L_0 \mp r\sin\theta(k)) + p_i^{b_2}, \forall i \in \mathcal{I}$.

When the joint torque τ generated by the two PAMs is given by $\tau(k) = r\cos\theta(k)(F_1(k) - F_2(k))$, the joint stiffness K_P is defined as the partial differentiation of joint torque τ by joint angle θ as follows [17]:

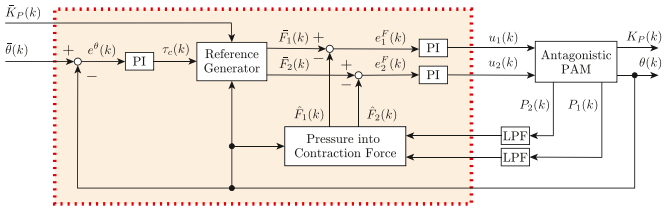

Fig. 2. Block diagram of angle-stiffness control system.

$$K_P(k) = r\sin\theta(k)(F_1(k) - F_2(k)) + r^2\cos^2\theta(k)\left(\frac{F_1(k) - \alpha_1(k)}{l_1(k)} + \frac{F_2(k) - \alpha_2(k)}{l_2(k)}\right) \quad (2)$$

where $\alpha_i(k) := p_i^{a_2} P_i(k) + p_i^{b_2}, \forall i \in \mathcal{I}$.

C. Angle-Stiffness Controller

This study proposes a nonlinear controller for the simultaneous control of joint angle and stiffness, which is highlighted in red in Fig. 2, as follows:

$$x(k+1) = A(k;\theta)x(k) + g(k;\zeta) \quad (3a)$$

$$\begin{bmatrix} u_1(k) \\ u_2(k) \end{bmatrix} = C(k;\theta)x(k) + h(k;\zeta) + \begin{bmatrix} \beta_1 \\ \beta_2 \end{bmatrix} \quad (3b)$$

where $x \in \mathbb{R}^3$ is the state, u_1 and $u_2 \in \mathbb{R}$ are the outputs of the controller, which are also the control inputs to the PDCVs, and $\zeta \in \mathbb{R}^5$ is the input, denoted by $\zeta := [\, P_1 \;\; P_2 \;\; \theta \;\; \bar{\theta} \;\; \bar{K}_P \,]^{\mathrm{T}}$, where P_1, P_2, and θ can be measured by the sensor, and $\bar{\theta}$ and $\bar{K}_P$ are the references. β_1 and β_2 are the bias voltages of each PDCV. $A(\theta) \in \mathbb{R}^{3\times3}$ and $C(\theta) \in \mathbb{R}^{2\times3}$ are time-varying, θ-dependent coefficients, and $g : \mathbb{R}^5 \to \mathbb{R}^3$ and $f : \mathbb{R}^5 \to \mathbb{R}^3$ are nonlinear functions of ζ. The coefficients and nonlinear functions are clarified after introducing a reference generator, pressure into the contraction force, and PI controllers, which are components of the proposed controller and are explained as follows.

1) Reference Generator: The reference generator outputs the reference signals of the contraction force for two PAMs, denoted as $\bar{F}_1$ and $\bar{F}_2$, taking the measured joint angle θ, computed torque command τ_c, and the given reference of joint stiffness $\bar{K}_P$ as inputs. Using [17], $\bar{F}_1$ and $\bar{F}_2$ are expressed as rational polynomial functions of the inputs θ, τ_c, and $\bar{K}_P$

$$\bar{F}_1(k) = \frac{1}{r^2\cos^2\theta(k)}\frac{l_1(k)l_2(k)}{l_1(k)+l_2(k)}\left[\bar{K}_P(k) + \left(\frac{r\cos\theta(k)}{l_2(k)} - \tan\theta(k)\right)\tau_c(k) - r^2\cos^2\theta(k)\left(\frac{\alpha_1(k)}{l_1(k)} + \frac{\alpha_2(k)}{l_2(k)}\right)\right] \quad (4a)$$

$$\bar{F}_2(k) = \bar{F}_1(k) - \frac{\tau_c(k)}{r\cos\theta(k)}. \quad (4b)$$

2) Pressure Into Contraction Force: The pressure-to-contraction force block shown in Fig. 2 estimates the contraction

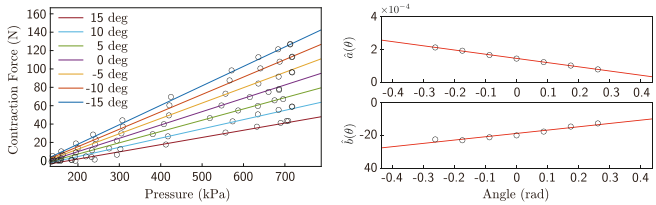

Fig. 3. Fitting result of the θ-dependent model (5) for capturing static characteristics with regard to P, F, and θ of the PAMs. (a) P–F relationship of the PAM. (b) $\hat{a}$–θ and $\hat{b}$–θ relationships of the PAM.

force of the PAM using the following experimental polynomial function of the inner pressure and measured joint angle:

$$\hat{F}_i(\theta(k), P_i(k)) = \hat{a}_i(\theta(k))P_i(k) + \hat{b}_i(\theta(k)) \tag{5a}$$

$$\hat{a}_i(\theta) = p_i^{\hat{a}_1}\theta + p_i^{\hat{a}_2}, \quad \hat{b}_i(\theta) = p_i^{\hat{b}_1}\theta + p_i^{\hat{b}_2} \tag{5b}$$

where $\hat{F}_i$, $\hat{a}_i$, and $\hat{b}_i$, $\forall i \in \mathcal{I}$, are an estimate of the PAM contraction force and the coefficients of (5a), respectively.

A reason for introducing the contraction force model (5) in addition to (1) is to reduce the number of approximation, which will facilitate the discussion in Section III. Model (1) involves a nonlinear term $\sin\theta$, which requires the approximation process to be a polynomial. On the other hand, model (5) is a polynomial of θ and captures a static relationship between the angle and the contraction force. Indeed, the fitting results of (5) are shown in Fig. 3. In Fig. 3(a), the black circles represent experimentally measured data, and the colored lines represent fitting results using (5) for each angle. In this case, the coefficients (5b) for each angle correspond to Fig. 3(b), where the black circles represent the coefficients corresponding to the colored lines in Fig. 3(a). The fitting test confirms that the θ-dependent model (5) is valid. Indeed, the numerical investigation that compares model (1) with its approximation (5) resulted in an error of less than 1.0 %, where the details are omitted here due to page limitation.

3) PI Controller: To compensate for errors in the joint angle and the contraction force, the proposed controller includes two types of PI controllers. The controller for the joint angle uses a feedback error between $\bar{\theta}$ and θ, denoted by $e^\theta := \bar{\theta} - \theta$, to compute the command torque τ_c, as follows:

$$\begin{bmatrix} x^\theta(k+1) \\ \tau_c(k) \end{bmatrix} = \begin{bmatrix} 1 & T_s \\ G_{\mathrm{I}}^\theta & G_{\mathrm{P}}^\theta \end{bmatrix} \begin{bmatrix} x^\theta(k) \\ e^\theta(k) \end{bmatrix} \tag{6}$$

where x^θ is the state and G_{P}^θ and G_{I}^θ are the proportional and integral gains, respectively.

Regarding the contraction force controller, the outputs of the reference generator, $\bar{F}_1$ and $\bar{F}_2$, are compared with the estimated forces $\hat{F}_1$ and $\hat{F}_2$ computed by (5), respectively. The resulting errors are fed to the PI controllers to generate the control input voltages u_1 and u_2 for each PDCV. The controllers are given as follows:

$$\begin{bmatrix} x_i^F(k+1) \\ u_i(k) \end{bmatrix} = \begin{bmatrix} 1 & T_s & 0 \\ G_{\mathrm{I}}^F & G_{\mathrm{P}}^F & 1 \end{bmatrix} \begin{bmatrix} x_i^F(k) \\ e_i^F(k) \\ \beta_i \end{bmatrix} \quad \forall i \in \mathcal{I} \tag{7}$$

where $x_i^F \forall i \in \mathcal{I}$, is the state of the ith controller, $e_i^F := \bar{F}_i - \hat{F}_i \forall i \in \mathcal{I}$, is the error in the contraction force of the ith PAM, G_{P}^F and G_{I}^F are the proportional and integral gains, respectively, and the gains are common between the controllers. In addition, we set the bias voltages β_1 and β_2 to 5.0 in the PDCVs.

Consequently, defining the controller state by $x := [\, x^\theta \;\; x_1^F \;\; x_2^F \,]^{\mathrm{T}}$ and eliminating τ_c, e^θ, e_i^F, $\bar{F}_i$, and $\hat{F}_i$ $\forall i \in \mathcal{I}$ from (4) to (7) results in the nonlinear controller (3) with the coefficients and functions in (8) shown at the bottom of the next page.

D. Numerical Verification

This section presents the numerical simulations conducted to evaluate the proposed nonlinear controller in terms of the control performance with respect to simultaneous angle-stiffness control. For the simulations, we used the following state-space model of an antagonistic PAM system [34]: $x_p(k+1) = f_\sigma(x_p(k), u(k))$ if $x_p(k) \in \mathcal{X}_\sigma$ holds, $y(k) = h_p(x_p(k))$, where $u := [u_1 \; u_2]^{\mathrm{T}} \in [0, 10]^2 \subset \mathbb{R}^2$ is the input voltages (V) to the two PDCVs, the state variable is $x_p := [\, \theta \;\; \dot{\theta} \;\; P_1 \;\; P_2 \,]^{\mathrm{T}} \in \mathbb{R}^4$, and the output variable is $y := [\, \theta \;\; P_1 \;\; P_2 \;\; K_P \,]^{\mathrm{T}} \in \mathbb{R}^4$, in which a set of allowable absolute pressures (kPa) is determined by the specification of the PAMs, i.e., $P_1, P_2 \in [200, 750]$, $f_\sigma : \mathbb{R}^4 \to \mathbb{R}^4$ is a nonlinear function with 18 subsystems, and it switches according to IF–THEN rules, $\mathcal{X}_\sigma := \{x_p \in \mathbb{R}^4 \mid \Psi_\sigma(x_p) > 0\}$ is the state set, where $\sigma \in \{1, 2, \ldots, 18\}$ is the index of the subsystem, $\Psi_\sigma(x_p)$ is a function derived from the modes in the form of IF–THEN rules, and the function $h_p : \mathbb{R}^4 \to \mathbb{R}^4$ is an observation equation.

We considered four types of references of the joint angle and stiffness. Reference 1 was set to

$$(\bar{\theta}(k), \bar{K}_P(k)) = \begin{cases} (10, 8) & \text{if } 0 \le T_s k < 15 \\ (10, 6) & \text{if } 15 \le T_s k < 30 \\ (10, 4) & \text{if } 30 \le T_s k < 45. \end{cases}$$

Reference 2 was set to

$$(\bar{\theta}(k), \bar{K}_P(k)) = \begin{cases} (5, 9) & \text{if } 0 \le T_s k < 15 \\ (15, 6) & \text{if } 15 \le T_s k < 30 \\ (10, 7) & \text{if } 30 \le T_s k < 45 \end{cases}$$

and References 3 and 4 were set to $(\bar{\theta}(k), \bar{K}_P(k)) = (15\sin(\frac{2\pi}{3}T_s k), 5)$ and $(15\sin(\frac{2\pi}{7.5}T_s k), 5)$ for $0 \le T_s k < 45$, respectively. The parameters of the PI controllers in (6) and (7) were determined by trial and error, resulting in $G_{\mathrm{P}}^\theta = 1.3$, $G_{\mathrm{I}}^\theta = 0.243$, $G_{\mathrm{P}}^F = 0.088$, and $G_{\mathrm{I}}^F = 0.025$. The initial voltage commands $u_1(0) = u_2(0) = 5.5$ were given before the start of the control, and the control was started after sufficient time had elapsed. In addition, note that the simulation results regarding

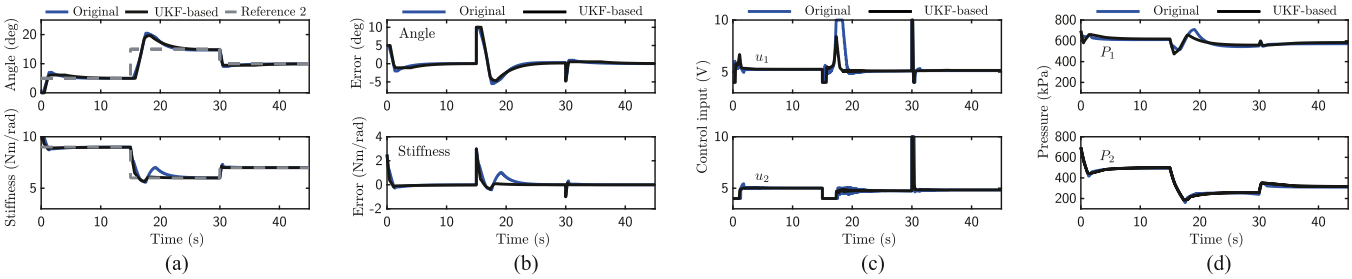

Fig. 4. Simulation results of the original and unscented Kalman filter (UKF)-based [17] simultaneous controls of joint angle and stiffness for Reference 2. (a) Joint angle and stiffness, (b) tracking errors of the joint angle and stiffness, (c) control inputs to the valve, and (d) inner pressure of each PAM.

References 1, 3, and 4 and experimental ones regarding References 1 and 3 have been omitted, and the results are discussed in Section IV-C owing to page limitations.

The simulation results of the proposed controller for Reference 2 are provided in Fig. 4, compared to the conventional unscented Kalman filter (UKF)-based simultaneous control method [17] to discuss the advantage of this study. In the figures, (a) shows the time response of the joint angle and stiffness, (b) presents the tracking errors of the joint angle and stiffness, (c) depicts the control inputs to the valve, and (d) shows the inner pressure of each PAM. The blue and black lines indicate the proposed and UKF-based controls, respectively. Fig. 4(a) and (b) confirms that the joint angle and stiffness track the reference in a steady state. In this case, the input voltages are saturated and oscillated in a transient state, as shown in Fig. 4(c). The operating pressure behavior is shown in Fig. 4(d). These results confirm that both the controllers achieve simultaneous tracking control of the joint angle and stiffness of the PAM actuator system. In addition, it was observed that the oscillations were influenced by the controller gains. Therefore, we tuned them to balance good tracking performance with oscillation reduction. Meanwhile, the UKF-based controller incorporates Coulomb friction and fluid dynamics nonlinearities explicitly, contributing to oscillation reduction.

However, the coefficients and input functions in the proposed controller are rational functions, which makes them difficult to be implemented in a controller device in an encrypted control fashion. In addition, the UKF-based control method cannot be applied to the controller encryption, as detailed in Remark 2. Therefore, in the following section, we consider the polynomial approximation of the proposed controller.

Remark 2: The proposed controller (3) is the use of the θ-dependent contraction force model (5), compared to the UKF-based controller achieving better performance, as shown in Fig. 4. The UKF-based controller involving fluid dynamics [17] and sliding-mode controllers [13], [14] include an IF–THEN rule; therefore, obtaining an alternative controller in a polynomial is difficult. Meanwhile, the nonlinear controllers proposed in [12], [15], and [16] can be applied to a polynomial approximation, whereas costly force sensors are required to measure the contraction force.

III. Polynomial Approximation of the Controller

This section presents the approximation of the proposed controller into polynomial functions and investigates the impact of the approximation on the response of the experimental PAM control system.

$$A(k;\theta) = \begin{bmatrix} 1 & 0 & 0 \\ \frac{T_s G_{\mathrm{I}}^{\theta} l_1(k) l_2(k)}{r^2 (l_1(k)+l_2(k)) \cos^2\theta(k)} \left(\frac{r\cos\theta(k)}{l_2(k)} - \tan\theta(k) \right) & 1 & 0 \\ T_s G_{\mathrm{I}}^{\theta} \left\{ \frac{l_1(k) l_2(k)}{r^2 (l_1(k)+l_2(k)) \cos^2\theta(k)} \left(\frac{r\cos\theta(k)}{l_2(k)} - \tan\theta(k) \right) - \frac{1}{r\cos\theta(k)} \right\} & 0 & 1 \end{bmatrix}, \quad g(k;\zeta) = T_s \begin{bmatrix} \bar{\theta}(k) - \theta(k) \\ h_1(k;\zeta) \\ h_2(k;\zeta) \end{bmatrix} \tag{8a}$$

$$C(k;\theta) = \begin{bmatrix} G_{\mathrm{P}}^F G_{\mathrm{I}}^{\theta} & G_{\mathrm{I}}^F & 0 \\ G_{\mathrm{P}}^F G_{\mathrm{I}}^{\theta} \left\{ \frac{l_1(k) l_2(k)}{r^2 (l_1(k)+l_2(k)) \cos^2\theta(k)} \left(\frac{r\cos\theta(k)}{l_2(k)} - \tan\theta(k) \right) - \frac{1}{r\cos\theta(k)} \right\} & 0 & G_I^F \end{bmatrix}, \quad h(k;\zeta) = G_{\mathrm{P}}^F \begin{bmatrix} h_1(k;\zeta) \\ h_2(k;\zeta) \end{bmatrix} \tag{8b}$$

$$h_1(k;\zeta) := \frac{l_1(k) l_2(k)}{l_1(k)+l_2(k)} \left[\frac{1}{r^2\cos^2\theta(k)} \left\{ -\bar{K}_P(k) + G_{\mathrm{P}}^{\theta} \left(\frac{r\cos\theta(t)}{l_2(k)} - \tan\theta(k) \right) (\bar{\theta}(k) - \theta(k)) \right\} + \frac{\alpha_1(k)}{l_1(k)} + \frac{\alpha_2(k)}{l_2(k)} \right] - \hat{a}_1 P_1(k) - \hat{b}_1 \tag{8c}$$

$$h_2(k;\zeta) := \frac{l_1(k) l_2(k)}{l_1(k)+l_2(k)} \left[\frac{1}{r^2\cos^2\theta(k)} \left\{ -\bar{K}_P(k) + G_{\mathrm{P}}^{\theta} \left(\frac{r\cos\theta(k)}{l_2(k)} - \tan\theta(k) - \frac{l_1(k)+l_2(k)}{l_1(k) l_2(k)} r\cos\theta(k) \right) (\bar{\theta}(k) - \theta(k)) \right\} + \frac{\alpha_1(k)}{l_1(k)} + \frac{\alpha_2(k)}{l_2(k)} \right] - \hat{a}_2 P_2(k) - \hat{b}_2 \tag{8d}$$

A. Controller Approximation

This study uses one- and two-variable functions to approximate the reference generator (4) in polynomials because only the reference generator is a rational function. By introducing five functions denoted by $f_1, \ldots, f_5$, let the rational functions (4) be rewritten as follows: $\bar{F}_1(k) = f_1(k;\theta,\bar{K}_P) + f_2(k;\theta)\tau_c(k) + f_3(k;\theta,P_1) + f_4(k;\theta,P_2)$, $\bar{F}_2(k) = \bar{F}_1(k) + f_5(k;\theta)\tau_c(k)$, where

$$
\begin{aligned}
f_1(k;\theta,\bar{K}_P) :=& -\frac{l_1(k)l_2(k)\bar{K}_P(k)}{r^2(l_1(k)+l_2(k))\cos^2\theta(k)} \\
f_2(k;\theta) :=& \frac{l_1(k)l_2(k)}{r^2(l_1(k)+l_2(k))\cos^2\theta(k)} \\
&\left(\frac{r\cos\theta(k)}{l_2(k)} - \tan\theta(k)\right) \\
f_3(k;\theta,P_1) :=& \frac{\alpha_1(P_1(k))l_2(k)}{l_1(k)+l_2(k)} \\
f_4(k;\theta,P_2) :=& \frac{\alpha_2(P_2(k))l_1(k)}{l_1(k)+l_2(k)}, \quad f_5(k;\theta) := -\frac{1}{r\cos\theta(k)}.
\end{aligned}
$$

For the five functions, we used the LASSO-based polynomial approximation [33] and manually removed coefficients with relatively small values, which resulted in the following approximated functions:

$$
\begin{aligned}
f_1(k;\theta,\bar{K}_P) &\approx w_1\bar{K}_p(k) + w_2\theta^2(k)\bar{K}_P(k) + w_3 =: \hat{f}_1 \\
f_2(k;\theta) &\approx w_4\theta(k) + w_5\theta^2(k) + w_6 =: \hat{f}_2 \\
f_3(k;\theta,P_1) &\approx w_7P_1(k) + w_8\theta(k)P_1(k) \\
&\quad + w_s\theta(k)P_1^2(k) + w_9 \\
&\approx w_7P_1(k) + w_8\theta(k)P_1(k) + w_9 =: \hat{f}_3 \\
f_4(k;\theta,P_2) &\approx w_{10}P_2(k) + w_{11}\theta(k)P_2(k) + w_{12} =: \hat{f}_4 \\
f_5(k;\theta) &\approx w_{13}\theta^2(k) + w_{14} =: \hat{f}_5
\end{aligned}
$$

where w_i, $\forall i \in \{1,2,\ldots,14\}$ and w_s are coefficients of approximated polynomials $\hat{f}_j$, $\forall j \in \{1,2,\ldots,5\}$, and their values are listed in Table II, where the regularization parameter of LASSO was set to 1.0. $\hat{f}_2$ and $\hat{f}_5$ are cubic polynomials in θ, and the other functions are cubic in both arguments. Furthermore, w_s of $\hat{f}_3$ resulted in a nonzero term, but it was significantly small compared to the other coefficients; thus, we removed w_s.

Consequently, we obtained the polynomial controller in (3) using the approximated coefficient matrices and functions specified as follows:

$$
A(k;\theta) \approx \begin{bmatrix} 1 & 0 & 0 \\ T_sG_{\mathrm{I}}^{\theta}\hat{f}_2(k;\theta) & 1 & 0 \\ T_sG_{\mathrm{I}}^{\theta}(\hat{f}_2(k;\theta)+\hat{f}_5(k;\theta)) & 0 & 1 \end{bmatrix} \tag{9a}
$$

$$
C(k;\theta) \approx \begin{bmatrix} G_{\mathrm{P}}^{F}G_{\mathrm{I}}^{\theta}\hat{f}_2(k;\theta) & G_{\mathrm{I}}^{F} & 0 \\ G_{\mathrm{P}}^{F}G_{\mathrm{I}}^{\theta}(\hat{f}_2(k;\theta)+\hat{f}_5(k;\theta)) & 0 & G_{\mathrm{I}}^{F} \end{bmatrix} \tag{9b}
$$

TABLE II
LIST OF PARAMETERS IN APPROXIMATED CONTROLLER

w_1	-61.7	$p_1^{a_1}$	7.05×10^{-3}
w_2	-1.89×10^{-2}	$p_1^{a_2}$	-1.02×10^{-4}
w_3	-1.58	$p_1^{b_1}$	-5.57×10^{2}
w_4	13.6	$p_1^{b_2}$	72.86
w_5	-1.24	$p_2^{a_1}$	6.42×10^{3}
w_6	1.73×10^{-3}	$p_2^{a_2}$	-9.18×10^{-4}
w_7	-5.12×10^{-1}	$p_2^{b_1}$	-1.98×10^{2}
w_8	-1.18×10^{-3}	$p_2^{b_2}$	15.75
w_s	-5.76×10^{-7}	$p_1^{a_1}$	-2.55×10^{-4}
w_9	36.5	$p_1^{a_2}$	1.45×10^{-4}
w_{10}	-4.31×10^{-1}	$p_1^{b_1}$	20.14
w_{11}	1.54×10^{-3}	$p_1^{b_2}$	-19.01
w_{12}	-9.35	$p_2^{a_1}$	2.18×10^{-4}
w_{13}	-27.3	$p_2^{a_2}$	1.45×10^{-4}
w_{14}	-3.92×10^{-3}	$p_2^{b_1}$	1.35
G_{P}^{θ}	1.3	$p_2^{b_2}$	-18.67
G_{I}^{θ}	2.43×10^{-1}	G_{I}^{F}	2.50×10^{-2}
G_{P}^{F}	8.80×10^{-2}		

$$
\begin{aligned}
h_1(k;\zeta) \approx\ & \hat{f}_1(k;\theta,\bar{K}_P) + G_{\mathrm{P}}^{\theta}\hat{f}_2(k;\theta)(\bar{\theta}(k)-\theta(k)) \\
& + \hat{f}_3(k;\theta,P_1) + \hat{f}_4(k;\theta,P_2) - \hat{a}_1P_1(k) - \hat{b}_1
\end{aligned} \tag{9c}
$$

$$
\begin{aligned}
h_2(k;\zeta) \approx\ & \hat{f}_1(k;\theta,\bar{K}_P) + \hat{f}_3(k;\theta,P_1) + \hat{f}_4(k;\theta,P_2) \\
& + G_{\mathrm{P}}^{\theta}(\hat{f}_2(k;\theta)+\hat{f}_5(k;\theta))(\bar{\theta}(k)-\theta(k)) \\
& - \hat{a}_2P_2(k) - \hat{b}_2.
\end{aligned} \tag{9d}
$$

B. Evaluation of Approximation Impacts

The impact of the controller approximation on the control performance is evaluated by comparing the experimental time responses of the control systems using the original controller (8) and the approximated controller (9). The scenarios of the control experiments are simultaneous tracking control of the joint angle and stiffness with and without a load. The references of the joint angle and stiffness set in the experiments are the same as those employed in the simulations. The experimental procedure without a load is as follows:

1) give the initial voltage commands $u_1(0) = u_2(0) = 5.5$ until sufficient time 30 s has elapsed;
2) start control with the original or approximated controller for each reference;
3) after the control, the measured angle and pressures, calculated stiffness, and control inputs are saved.

The experimental results for the original and approximated controllers without a load are shown in Figs. 5 and 6. In this figure, the blue and red lines indicate the results of the original and approximated control systems, respectively, and their meanings are the same as those in Fig. 4. Figs. 5(a) and (b) and 6(a) and (b) confirm that the angle and stiffness track the reference in the steady state and that sufficient control performance is maintained. The polynomial controller exhibits similar overshoot compared to the original controller due to the

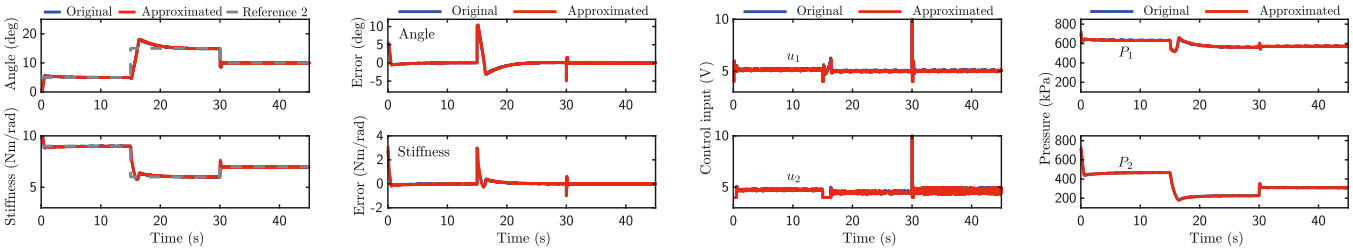

Fig. 5. Comparison of experimental results of original and approximated polynomial load-free controls of joint angle and stiffness for Reference 2. (a) Joint angle and stiffness. (b) Tracking errors of the joint angle and stiffness. (c) Control inputs to the valve. (d) Inner pressure of each PAM.

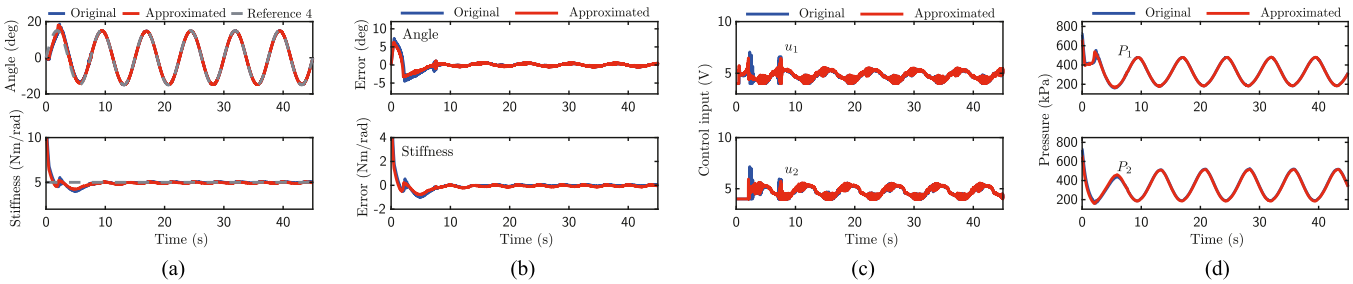

Fig. 6. Comparison of experimental results of original and approximated polynomial load-free controls of joint angle and stiffness for Reference 4. (a) Joint angle and stiffness. (b) Tracking errors of the joint angle and stiffness. (c) Control inputs to the valve. (d) Inner pressure of each PAM.

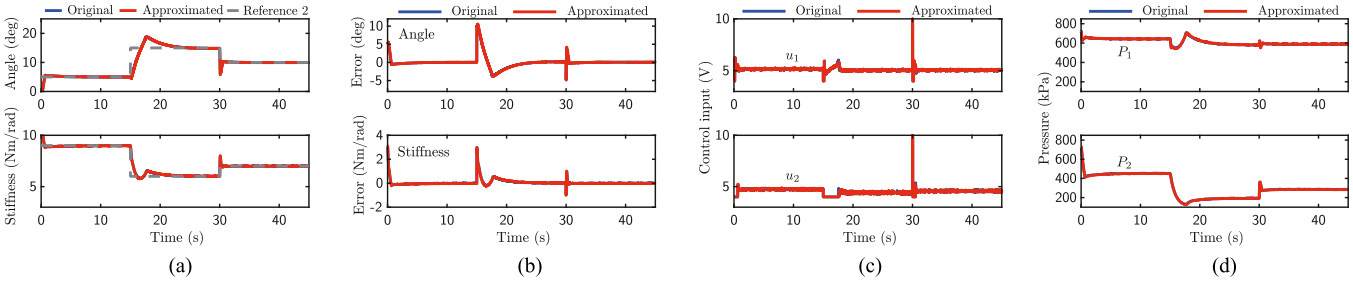

Fig. 7. Comparison of experimental results of original and approximated polynomial controls with load for Reference 2. (a) Joint angle and stiffness. (b) Tracking errors of the joint angle and stiffness. (c) Control inputs to the valve. (d) Inner pressure of each PAM.

approximation. Figs. 5(c) and (d); 6(c) and (d) observe that the experimental results of the original and approximated controllers exhibit similar behavior in the steady state. In addition, the input saturation occurs at 30 s, whereas it does not affect the tracking control performance in the steady state.

Moreover, we conducted a control experiment, wherein a 1.5 kg load was hung from the left side of the joint before starting control to evaluate the impact of the approximation. The experimental procedure with a load is as follows:

i) give the initial voltage commands $u_1(0) = u_2(0) = 5.5$ until sufficient time 30 s has elapsed;
ii) hang a 1.5 kg load from the left side of the joint and perform Step i);
iii) start control with the original or approximated controller for each reference;
iv) after the control, the measured angle and pressures, calculated stiffness, and control inputs are saved.

The experimental results with the load are shown in Figs. 7 and 8, where the line colors in each figure are the same as those in Fig. 5. Figs. 7(a) and (b); 8(a) and (b) confirm that the angle and stiffness track the reference in the steady state. Good control tracking causes the controller to compensate for the impact of the load, which can be observed as a difference of approximately 50 kPa over the steps between the responses of the inner pressures, as shown in Figs. 5(d) and 7(d) for Reference 2 and Figs. 6(d) and 8(d) for Reference 4. Similarly, Figs. 7(c) and 8(c) demonstrate that the experimental results of the two controllers exhibit similar behaviors in the steady state, respectively. Fig. 7(c) confirms that the input saturation occurs at 30 s, which does not affect the control performance.

The experimental results confirm that the approximated controller achieves almost the same control performance as that of the original controller, implying that the impact of the controller approximation is negligible. Therefore, the original controller

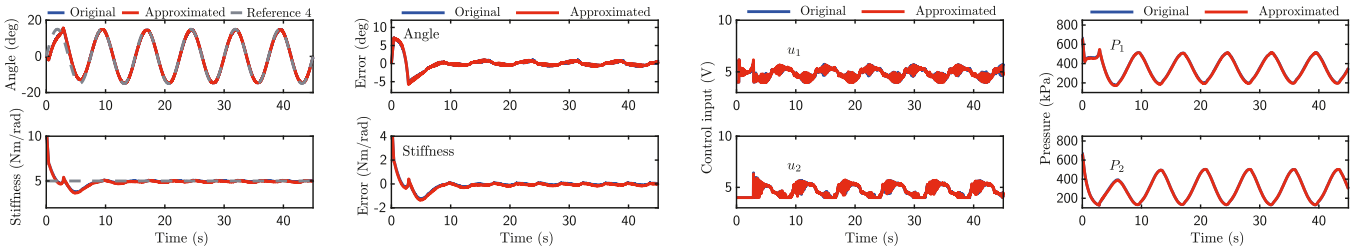

Fig. 8. Comparison of experimental results of original and approximated polynomial controls with load for Reference 4. (a) Joint angle and stiffness. (b) Tracking errors of the joint angle and stiffness. (c) Control inputs to the valve. (d) Inner pressure of each PAM.

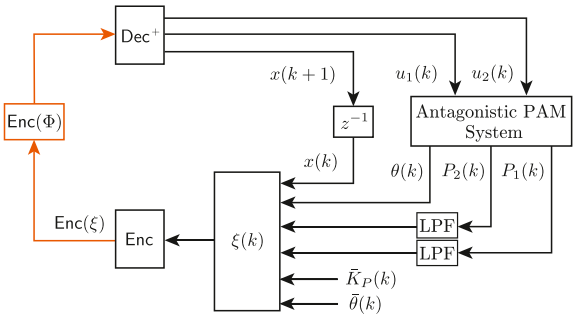

Fig. 9. Encrypted angle and stiffness control system.

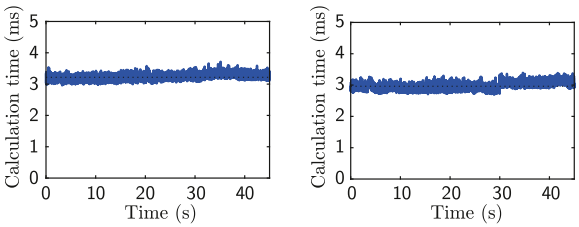

Fig. 10. Processing time: less than the sampling period of 4.0 ms. (a) Reference 2 without load. (b) Reference 2 with load.

can be replaced with an approximated controller that is adequate for secure implementation.

IV. Secure PAM Actuator With Encrypted Polynomial-Type Controller

This section demonstrates the developed encrypted simultaneous control system for an antagonistic PAM actuator. The control system employs the controller encryption [26] to be secure, maintaining the control performance.

A. Secure Implementation

The controller encryption method can make a linear control operation in a matrix-vector product form confidential. Hence, we consider to transform our proposed polynomial controller into a product of matrix and vector. In this study, by defining a vector of monomials as $\xi \in \mathbb{R}^{18}$, the polynomial controller (3) with the coefficients and functions (9) can be transformed into the following matrix-vector multiplication:

$$\psi(k) = \Phi\xi(k) \quad \forall k \in \mathbb{Z}^+ \tag{10}$$

with $\xi := [\,\bar{K}_P \;\; \bar{K}_P\theta^2 \;\; \bar{\theta} \;\; \theta \;\; x^\theta \;\; \bar{\theta}\theta \;\; \theta^2 \;\; x^\theta\theta \;\; \bar{\theta}\theta^2 \;\; \theta^3 \;\; x^\theta\theta^2 \;\; P_1 \;\; \theta P_1 \;\; P_2 \;\; \theta P_2 \;\; 1 \;\; x_1^F \;\; x_2^F\,]^{\mathrm{T}}$, $\psi(k) := [\,x^\theta(k+1) \;\; x_1^F(k+1) \;\; x_2^F(k+1) \;\; u_1(k) \;\; u_2(k)\,]^{\mathrm{T}}$, where ξ and $\psi \in \mathbb{R}^5$ are the input and output of the encrypted controller, respectively. The coefficient matrix $\Phi \in \mathbb{R}^{5\times 18}$ is given as follows:

$$\Phi = \begin{bmatrix}
0 & 0 & T_s & -T_s & 1 & 0 \\
T_s w_1 & T_s w_2 & T_s\phi_3 & T_s\phi_4 & T_s\phi_5 & T_s\phi_6 \\
T_s w_1 & T_s w_2 & T_s\nu_3 & T_s\nu_4 & T_s\nu_5 & T_s\nu_6 \\
G_P^F w_1 & G_P^F w_2 & G_P^F\phi_3 & G_P^F\phi_4 & G_P^F\phi_5 & G_P^F\phi_6 \\
G_P^F w_1 & G_P^F w_2 & G_P^F\nu_3 & G_P^F\nu_4 & G_P^F\nu_5 & G_P^F\nu_6
\end{bmatrix}$$

$$\begin{bmatrix}
0 & 0 & 0 & 0 & 0 & 0 \\
T_s\phi_7 & T_s\phi_8 & T_s\phi_9 & T_s\phi_{10} & T_s\phi_{11} & T_s\phi_{12} \\
G_P^F\phi_7 & G_P^F\phi_8 & G_P^F\phi_9 & G_P^F\phi_{10} & G_P^F\phi_{11} & T_s\nu_{12} \\
G_P^F\phi_7 & G_P^F\phi_8 & G_P^F\phi_9 & G_P^F\phi_{10} & G_P^F\phi_{11} & G_P^F\phi_{12} \\
G_P^F\nu_7 & G_P^F\nu_8 & G_P^F\nu_9 & G_P^F\nu_{10} & G_P^F\nu_{11} & G_P^F\nu_{12}
\end{bmatrix}$$

$$\begin{bmatrix}
0 & 0 & 0 & 0 & 0 & 0 \\
T_s\phi_{13} & T_s\phi_{14} & T_s\phi_{15} & T_s\phi_{16} & 1 & 0 \\
T_s\nu_{13} & T_s\nu_{14} & T_s\nu_{15} & T_s\nu_{16} & 0 & 1 \\
G_P^F\phi_{13} & G_P^F\phi_{14} & G_P^F\phi_{15} & G_P^F\phi_{16}+\beta_1 & G_I^F & 0 \\
G_P^F\nu_{13} & G_P^F\nu_{14} & G_P^F\nu_{15} & G_P^F\nu_{16}+\beta_2 & 0 & G_I^F
\end{bmatrix}$$

where $\phi_3 := w_4 G_P^\theta$, $\phi_4 := -p_1^{b_1} - w_4 G_P^\theta$, $\phi_5 := w_4 G_I^\theta$, $\phi_6 := w_5 G_P^\theta$, $\phi_7 := -w_5 G_P^\theta$, $\phi_8 := w_5 G_I^\theta$, $\phi_9 := w_6 G_P^\theta$, $\phi_{10} := -w_6 G_P^\theta$, $\phi_{11} := w_6 G_I^\theta$, $\phi_{12} := w_7 - p_2^{a_1}$, $\phi_{13} := w_8 - p_1^{\hat{a}_1}$, $\phi_{14} := w_{10}$, $\phi_{15} := w_{11}$, $\phi_{16} := w_3 + w_9 + w_{12} - p_2^{\hat{b}_1}$, $\nu_3 := (w_4 + w_{13}) G_P^\theta$, $\nu_4 := -p_1^{\hat{b}_2} - (w_4 + w_{13}) G_P^\theta$, $\nu_5 := (w_4 + w_{13}) G_I^\theta$, $\nu_6 := w_5 G_P^\theta$, $\nu_7 := -w_5 G_P^\theta$, $\nu_8 := w_5 G_I^\theta$, $\nu_9 := (w_6 + w_{14}) G_P^\theta$, $\nu_{10} := -(w_6 + w_{14}) G_P^\theta$, $\nu_{11} := (w_6 + w_{14}) G_I^\theta$, $\nu_{12} := w_7$, $\nu_{13} := w_8$, $\nu_{14} := w_{10} - p_2^{\hat{a}_2}$, $\nu_{15} := w_{11} - p_1^{\hat{a}_2}$, and $\nu_{16} := w_3 + w_9 + w_{12} - p_2^{\hat{b}_2}$. The augmented formulation of controller (10) is a linear operation; thus, the same procedure for encrypting a linear controller is applied to encrypt the controller, as described in [29]. The configuration of the control system is illustrated in Fig. 9, where the controller input ξ is generated by the reference signals, measurements, and states of the PI controllers. The input ξ is encrypted by using an ElGamal encryption scheme in the `Enc` block. The encrypted controller Enc(Φ) conducts multiplicative homomorphic operations, and

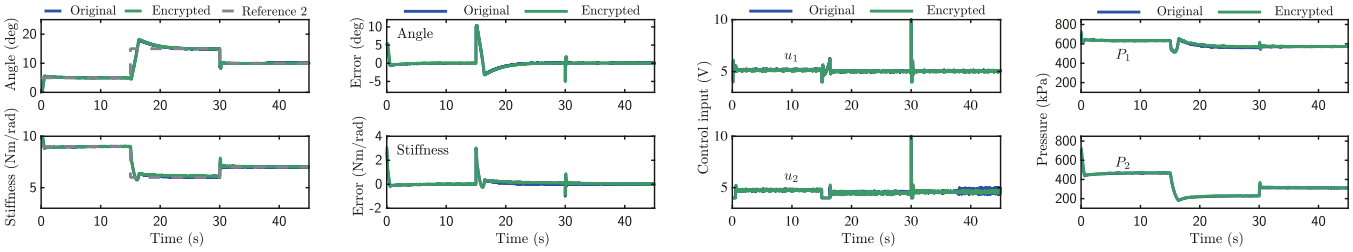

Fig. 11. Experimental results of unencrypted and encrypted simultaneous load-free control of joint angle and stiffness for Reference 2. (a) Joint angle and stiffness. (b) Tracking errors of the joint angle and stiffness. (c) Control inputs to the valve. (d) Inner pressure of each PAM.

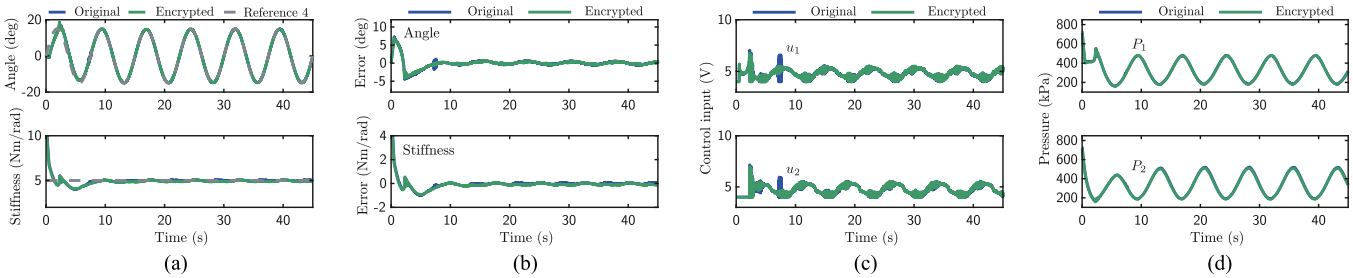

Fig. 12. Experimental results of unencrypted and encrypted simultaneous load-free control of joint angle and stiffness for Reference 4. (a) Joint angle and stiffness. (b) Tracking errors of the joint angle and stiffness. (c) Control inputs to the valve. (d) Inner pressure of each PAM.

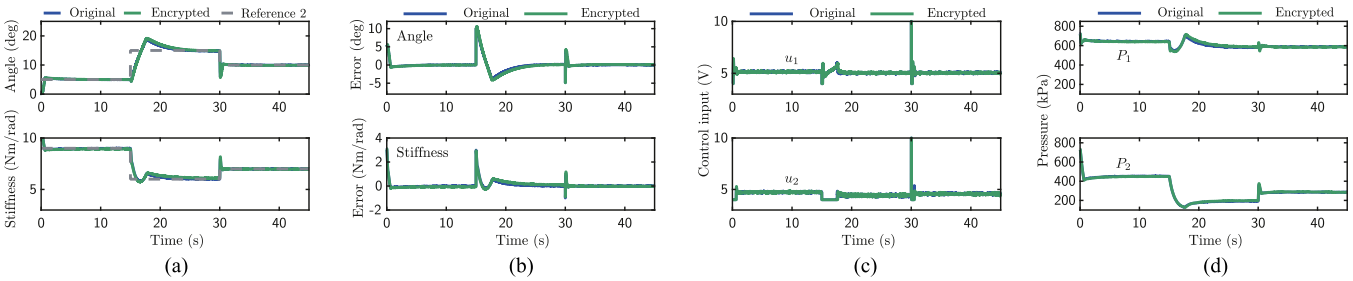

Fig. 13. Experimental results of unencrypted and encrypted simultaneous controls with load for Reference 2. (a) Joint angle and stiffness. (b) Tracking errors of the joint angle and stiffness. (c) Control inputs to the valve. (d) Inner pressure of each PAM.

Dec^{+} extracts the plaintext states and control inputs to each PDCV. For the notations regarding the encryption scheme, please refer to [26].

B. Experimental Validation

This section verifies the encrypted control system by comparing the experimental results obtained using the encrypted and original control systems. A key length of 64 b was chosen, and the scaling parameters Δ_ξ and Δ_Φ were set to 1.0×10^8, which were introduced in [26] to manage the quantization errors due to encryption.

The scenarios of the control experiments involve simultaneous tracking control of the joint angle and stiffness with and without the load. The references of the joint angle and stiffness were the same as those of the simulations in Fig. 4. The experimental procedures without and with a load is the same as one described in Section III-B, where the original or encrypted controller was used. The experimental results are shown in Figs. 11 and 14. In the figures, the blue and green lines represent the results of the original and encrypted control systems, respectively. Figs. 11(a) and (b); 14(a) and (b) confirm that the angle and stiffness track the reference in the steady state and that sufficient control performance is maintained. Figs. 11(c) and 13(c) confirm that the input saturation occurs, which does not affect the control performance. The destabilization caused by saturation should be analyzed, but it is difficult to address, so the stability analysis of the constrained PAM's actuator system will be tackled in the future. Similarly, they show that the controller compensated for the impact of the load, which can be observed as a difference of approximately 50 kPa, as shown in Figs. 11(d) and 13(d) for Reference 2 and Figs. 12(d) and 14(d) for Reference 4.

The computation time involved in the encrypted control system is shown in Fig. 10, where Fig. 10(a) and (b) correspond to Figs. 11 and 13. The figures show that the control operation is

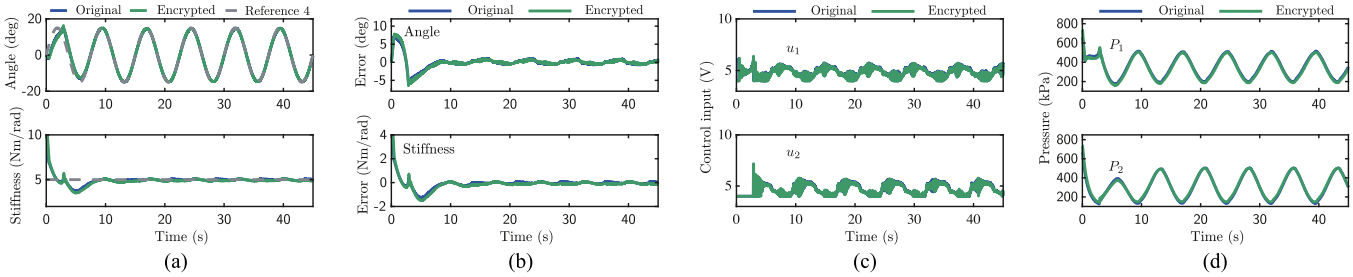

Fig. 14. Experimental results of unencrypted and encrypted simultaneous load-free control of joint angle and stiffness with load for Reference 4. (a) Joint angle and stiffness. (b) Tracking errors of the joint angle and stiffness. (c) Control inputs to the valve. (d) Inner pressure of each PAM.

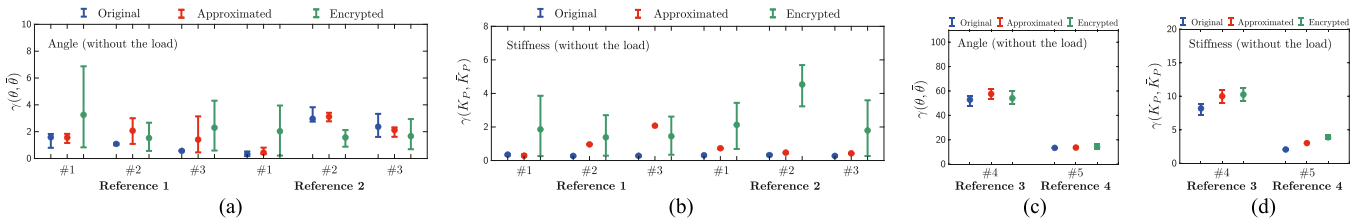

Fig. 15. ℓ_2-norm scores of the tracking errors of the (a) joint angle and (b) stiffness for Reference 2 and (c) joint angle and (d) stiffness for Reference 4 using the original, approximated, and encrypted controllers without a load.

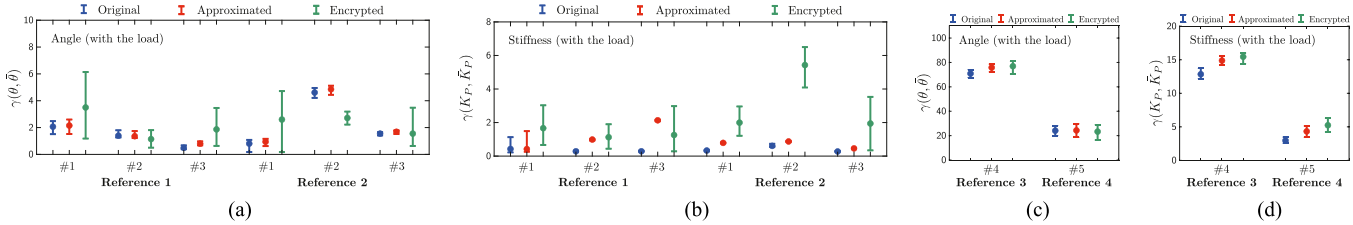

Fig. 16. ℓ_2-norm scores of the tracking errors of the (a) joint angle and (b) stiffness for Reference 2 and (c) joint angle and (d) stiffness for Reference 4 using the original, approximated, and encrypted controllers with a load.

in real time because the computation time for each step is less than the sampling period.

C. Quantitative Investigation

We quantitatively evaluate the control results presented so far to investigate the impact of the secure implementation of the nonlinear controller on the control performance. For this purpose, we introduce the ℓ_2 norm to measure the tracking error during a specific duration for each control result, as shown in Figs. 5–8 and 11–14. The ℓ_2 norm is defined as $\gamma(z,\bar{z}) := \sqrt{\sum_{k=k_0}^{k_1}(z(k)-\bar{z}(k))^2}$, where z and $\bar{z}$ represent scalar signal sequences, and the evaluation steps (closed interval) $[k_0, k_1]$ are set to [2500,3749], [6250,7499], [10 000,11 249], [10 500,11 249] and [9375,11 249]. These intervals are labeled #1, #2, and #3 in References 1 and 2 and #4 and #5 in References 3 and 4, respectively.

The ℓ_2-norm scores of the original, approximated, and encrypted controls with and without loads are summarized in Figs. 15 and 16, respectively. In each figure, (a) and (b) for References 1 and 2 and (c) and (d) for References 3 and 4 display $\gamma(\theta,\bar{\theta})$ and $\gamma(K_P,\bar{K}_P)$, respectively, for the corresponding evaluation steps. The blue, red, and green colors represent the ℓ_2-norm values of the original, approximated, and encrypted controllers, respectively. The dots and error bars indicate the average, maximum, and minimum ℓ_2-norm values from 10 experiments.

These figures confirm that the resulting scores tend to increase as the procedure advances through the polynomial approximation and secure implementation. However, in many cases, the scores of the original and encrypted controllers are similar. The worst rate of the controlled signal relative to step-like reference is $4.82/5.00 \times 100 = 96.3\,\%$ for #1 of Reference 1 in Fig. 15(a) and $6.22/6.00 \times 100 = 103.7\,\%$ for #2 of Reference 2 in Fig. 15(b). This result implies that the proposed encrypted control achieved a tracking error of less than 3.7% for the step-like references. Meanwhile, the worst rate to the sinusoidal reference is $9.38/14.9 \times 100 = 63.0\%$ for #4 of Reference 3 in Fig. 16(c) and $1.76/2.40 \times 100 = 73.3\%$ for #5 of Reference 4 in Fig. 15(c), which are relatively large compared to ones for step-like references. This degradation might cause the proposed controller not to satisfy an internal model principle,

which will be addressed in future work. In addition, Figs. 15(c) and (d); 16(c) and (d) confirm that better control performance for sinusoidal references with longer periods equal to or than 7.5 s was obtained.

Moreover, in cases where a relatively large change in the score occurs, such as #3 of Reference 1 in Figs. 15(a) and (b); 16(b), the effect of the polynomial approximation prevails over the change in. In other words, the change in score from blue to red is larger than that from red to green. This discussion provides further insight, suggesting that increasing the accuracy of the polynomial approximation could help avoid the degradation of the original control performance. It is crucial to consider an accuracy-aware approximation method suitable for secure implementation, which will be the focus of future work. In addition, these figures confirm that, owing to the lack of significant differences between the cases without and with the load, the proposed control system is capable of compensating for the unknown load.

V. Conclusion

This study proposed an encrypted simultaneous control system for antagonistic PAM actuators aimed at developing cyber-secure and safe PAM actuator systems. A nonlinear controller was designed to track the joint angle and stiffness simultaneously based on the PAM actuator model. By applying the polynomial approximation technique to a nonlinear controller, we obtained a polynomial-type controller. Subsequently, we developed a secure PAM actuator system through the secure implementation in the control device. For experimental validation, the ℓ_2 norm was introduced to measure and compare the experimental results of the original, approximated, and encrypted controllers. The experimental results showed that the proposed encrypted controller achieved simultaneous tracking of the joint angle and stiffness of the PAM actuator with a tracking error of less than 3.7 % for step-like reference. Consequently, the developed PAM actuator system, enabled by the secure implementation of the simultaneous controller, enhances security while maintaining a control performance similar to that of the original controller. The developed actuator is expected to be used in secure and safe PAM-driven devices, such as nursing care robots, rehabilitation orthoses, and power-assisted orthoses for remote usage applications.

In future work, we plan to further improve the control performance of the encrypted controller by addressing the nonlinear characteristics of PAMs, including Coulomb friction and fluid dynamics, and by applying a controller design based on the internal model principle under a sinusoidal reference. To mitigate the performance degradation caused by the polynomial approximation, we investigate more effective strategies for tuning the regularization parameter in LASSO. Moreover, when considering the secure implementation of cost-effective computers, reducing the computation time is essential to achieve a resource-aware encrypted controller by streamlining the proposed controller. Furthermore, verification against cyberattacks will be addressed to develop more practical and secure actuators.

References

[1] C.-P. Chou and B. Hannaford, "Measurement and modeling of McKibben pneumatic artificial muscles," *IEEE Trans. Robot. Autom.*, vol. 12, no. 1, pp. 90–102, Feb. 1996.

[2] D. G. Caldwell, G. A. Medrano-Cerda, and M. Goodwin, "Control of pneumatic muscle actuators," *IEEE Control Syst. Mag.*, vol. 15, no. 1, pp. 40–48, Feb. 1995.

[3] B. Tondu and P. Lopez, "Modeling and control of McKibben artificial muscle robot actuators," *IEEE Control Syst. Mag.*, vol. 20, no. 2, pp. 15–38, Apr. 2000.

[4] T. V. Minh, B. Kamers, T. Tjahjowidodo, H. Ramon, and H. Van Brussel, "Modeling torque-angle hysteresis in a pneumatic muscle manipulator," in *Proc. IEEE/ASME Int. Conf. Adv. Intell. Mechatron.*, 2010, pp. 1122–1127.

[5] G. Andrikopoulos, G. Nikolakopoulos, and S. Manesis, "Advanced nonlinear PID-based antagonistic control for pneumatic muscle actuators," *IEEE Trans. Ind. Electron.*, vol. 61, no. 12, pp. 6926–6937, Dec. 2014.

[6] G. Andrikopoulos, G. Nikolakopoulos, and S. Manesis, "A survey on applications of pneumatic artificial muscles," in *Proc. IEEE Mediterranean Conf. Control Autom.*, 2011, pp. 1439–1446.

[7] I. Sardellitti, G. Palli, N. G. Tsagarakis, and D. G. Caldwell, "Antagonistically actuated compliant joint: Torque and stiffness control," in *Proc. IEEE/RSJ Int. Conf. Intell. Robots Syst.*, 2010, pp. 1909–1914.

[8] L. M. Sui and S. Q. Xie, "A model of pneumatic muscle actuated joint using linearized method," in *Proc. IEEE 19th Int. Conf. Mechatron. Mach. Vis. Pract.*, 2012, pp. 414–419.

[9] B. Ugurlu, P. Forni, C. Doppmann, and J. Morimoto, "Torque and variable stiffness control for antagonistically driven pneumatic muscle actuators via a stable force feedback controller," in *Proc. IEEE/RSJ Int. Conf. Intell. Robots Syst.*, 2015, pp. 1633–1639.

[10] Y. Yamamoto, N. Matsunaga, and H. Okajima, "Robust variable stiffness control of McKibben type pneumatic artificial muscle arm by using multiple model error compensators," in *Proc. IEEE Int. Conf. Control Autom. Syst.*, 2017, pp. 957–962.

[11] X. Zhao, H. Ma, D. Ye, and D. Zhang, "Independent stiffness and force control of antagonistic pneumatic artificial muscles joint," in *Proc. IEEE Int. Conf. Adv. Robot. Mechatron.*, 2017, pp. 734–739.

[12] D. Tanaka, H. Maeda, and T. Nakamura, "Joint stiffness and position control of an artificial muscle manipulator considering instantaneous load," in *Proc. IEEE Annu. Conf. Ind. Electron.*, 2009, pp. 2259–2264.

[13] T. Y. Choi, B. S. Choi, and K. H. Seo, "Position and compliance control of a pneumatic muscle actuated manipulator for enhanced safety," *IEEE Trans. Control Syst. Technol.*, vol. 19, no. 4, pp. 832–842, Jul. 2011.

[14] J. Cao, S. Q. Xie, and R. Das, "MIMO sliding mode controller for gait exoskeleton driven by pneumatic muscles," *IEEE Trans. Control Syst. Technol.*, vol. 26, no. 1, pp. 274–281, Jan. 2018.

[15] N. Saito and T. Satoh, "Posture control considering joint stiffness of a robotic arm driven by rubberless artificial muscle," *Int. J. Autom. Technol.*, vol. 10, no. 4, pp. 503–510, 2016.

[16] B. Ugurlu, P. Forni, C. Doppmann, E. Sariyildiz, and J. Morimoto, "Stable control of force, position, and stiffness for robot joints powered via pneumatic muscles," *IEEE Trans. Ind. Informat.*, vol. 15, no. 12, pp. 6270–6279, Dec. 2019.

[17] T. Shin and K. Kogiso, "Sensorless angle and stiffness control of antagonistic PAM actuator using reference set," *Adv. Robot.*, vol. 36, no. 9, pp. 423–437, 2022.

[18] H. Li, K. Tadano, and K. Kawashima, "Achieving force perception in master-slave manipulators using pneumatic artificial muscles," in *Proc. IEEE SICE Annu. Conf.*, 2012, pp. 1342–1345.

[19] T. Sasaki, T. Nagai, and K. Kawashima, "Remote control of backhoe for rescue activities using pneumatic robot system," in *Proc. IEEE Int. Conf. Robot. Autom.*, 2006, pp. 3177–3182.

[20] T. Kato, T. Higashi, and K. Shimizu, "Teleoperation of a robot arm system using pneumatic artificial rubber muscles: Teleoperation over the internet using UDP and a web camera," in *Proc. IEEE Int. Conf. Broadband, Wireless Computing, Commun. Appl.*, 2010, pp. 714–718.

[21] H. Toda, M. Tada, T. Maruyama, and Y. Kurita, "Effect of contraction parameters on swing support during walking using wireless pneumatic artificial muscle driver: A preliminary study," in *Proc. IEEE 58th Annu. Conf. Soc. Instrum. Control Engineers*, 2019, pp. 727–732.

[22] S. Yean, M. Tada, H. Toda, B.-S. Lee, and Y. Kurita, "Adaptive automatic controller for swing assist by pneumatic artificial muscle," in *Proc. IEEE Sensors Appl. Symp.*, 2020, pp. 1–6.

[23] R. Langner, "Stuxnet: Dissecting a cyberwarfare weapon," *IEEE Secur. Privacy*, vol. 9, no. 3, pp. 49–51, May/Jun. 2011.
[24] S. Gorman, Y. J. Dreazen, and A. Cole, "Insurgents hack US drones," 2009. [Online]. Available: https://www.wsj.com/articles/SB126102247889095011
[25] D. Quarta, M. Pogliani, M. Polino, F. Maggi, A. M. Zanchettin, and S. Zanero, "An experimental security analysis of an industrial robot controller," in *Proc. IEEE Symp. Secur. Privacy*, 2017, pp. 268–286.
[26] K. Kogiso and T. Fujita, "Cyber-security enhancement of networked control systems using homomorphic encryption," in *Proc. IEEE Conf. Decis. Control*, 2015, pp. 6836–6843.
[27] K. Teranishi, K. Kogiso, and J. Ueda, "Encrypted feedback linearization and motion control for manipulator with somewhat homomorphic encryption," in *Proc. IEEE/ASME Int. Conf. Adv. Intell. Mechatron.*, 2020, pp. 613–618.
[28] Y. Qiu and J. Ueda, "Encrypted motion control of a teleoperation system with security-enhanced controller by deception," in *Proc. Dynamic Syst. Control Conf.*, 2019, Art. no. V001T07A006.
[29] T. Shin, K. Teranishi, and K. Kogiso, "Cyber-secure pneumatic actuator system equipped with encrypted controller and attack detectors," *Adv. Robot.*, vol. 36, no. 9, pp. 438–449, 2022.
[30] R. Baba, K. Kogiso, and M. Kishida, "Detection method of controller falsification attacks against encrypted control system," in *Proc. SICE Annu. Conf.*, 2018, pp. 244–248.
[31] M. Miyamoto, K. Teranishi, K. Emura, and K. Kogiso, "Cybersecurity-enhanced encrypted control system using keyed-homomorphic public key encryption," *IEEE Access*, vol. 11, pp. 45749–45760, 2023.
[32] M. Schulze Darup, "Encrypted polynomial control based on tailored two-party computation," *Int. J. Robust Nonlinear Control*, vol. 30, no. 11, pp. 4168–4187, 2020.
[33] Y. Takeda and K. Kogiso, "Experimental regularization parameter search for polynomial approximation of nonlinear PAM controller," in *Proc. IEEE/SICE Int. Symp. Syst. Integration*, 2023, pp. 1–6.
[34] T. Shin, T. Ibayashi, and K. Kogiso, "Detailed dynamic model of antagonistic PAM system and its experimental validation: Sensorless angle and torque control with UKF," *IEEE/ASME Trans. Mechatron.*, vol. 27, no. 3, pp. 1715–1726, Jun. 2022.

Yuta Takeda (Student Member, IEEE) received the B.S. degree in informatics and engineering in 2022 from The University of Electro-Communications, Tokyo, Japan, where he is currently working toward the M.S. degree in model-based analysis and design of pneumatic artificial muscle actuators.

His research interests include control applications and modeling/control of pneumatic artificial muscles.

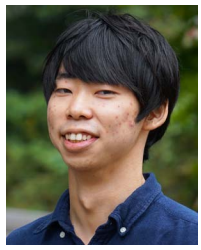

Takaya Shin received the B.S. and M.S. degrees in informatics and engineering from The University of Electro-Communications, Tokyo, Japan, in 2020 and 2022, respectively.

He joined Daihen Company, Osaka, Japan. His research interests include control applications and modeling/control of pneumatic artificial muscles.

Kaoru Teranishi (Student Member, IEEE) received the B.S. degree in electronic and mechanical engineering from the National Institute of Technology, Ishikawa College, Ishikawa, Japan, in 2019, and the M.S. and Ph.D. degrees in mechanical and intelligent systems engineering from the University of Electro-Communications, Tokyo, Japan, in 2021 and 2024, respectively.

From 2019 to 2020, he was a Visiting Scholar with the Georgia Institute of Technology, Atlanta, GA, USA. From 2021 to 2024, he was a Research Fellow of the Japan Society for the Promotion of Science, Tokyo, Japan. Since 2024, he has been a Postdoctoral Researcher with the University of Electro-Communications. His research interests include control theory and cryptography for control systems security.

Kiminao Kogiso (Member, IEEE) received the B.E., M.E., and Ph.D. degrees in mechanical engineering from Osaka University, Suita, Japan, in 1999, 2001, and 2004, respectively.

He was a Postdoctoral Fellow with the 21st Century COE Program and an Assistant Professor with the Graduate School of Information Science, Nara Institute of Science and Technology, Nara, Japan, in 2004 and 2005, respectively. From 2010 to 2011, he was a Visiting Scholar with the Georgia Institute of Technology, Atlanta, GA, USA. In 2014, he was promoted to Associate Professor with the Department of Mechanical and Intelligent Systems Engineering, The University of Electro-Communications, Tokyo, Japan. Since 2023, he has been a Professor with the same department. His research interests include the cybersecurity of control systems, constrained control, and control of decision-makers and their applications.